Article

Study on the Influence of an Internal Stiffening System on the Structural Strength of the Semi-Submersible Structures for a Floating Offshore Wind Turbine

Hao Yu Dou, Han Koo Jeong * and Jian Lun Jiang

Department of Naval Architecture and Ocean Engineering, Kunsan National University, Gunsan 54150, Republic of Korea; 2420119@kunsan.ac.kr (H.Y.D.); jiangjianlun@kunsan.ac.kr (J.L.J.)
* Correspondence: hkjeong@kunsan.ac.kr; Tel.: +82-63-469-1853

Abstract: This study presents the development and comparative analysis of a new Y-type floating offshore wind turbine platform based on the existing T-type model. Utilizing advanced simulation tools, such as MSC, Patran and Nastran 2022.3, FEGate For Ship 5.0, and Ansys AQWA 2021 R2, extensive evaluations are conducted on the structural strength, stability, and dynamic response of both the T-type and the newly proposed Y-type platforms. In this research, the structural optimization algorithm based on the above simulation tools is adopted, and its results are compared with preoptimization results to demonstrate the improvements made in design precision and reliability. Results indicate that the Y-type model achieves a maximum reduction in von Mises stress by 30.21 MPa compared to the T-type model, and its heave and pitch motion amplitudes are reduced by 4.3412 m and 4.9362°, respectively, under extreme sea state conditions. Through structural optimization using the Nastran SOL200 module, the column structure weight is reduced by 11.31%, meeting the strength requirements while enhancing efficiency. These findings highlight the Y-type platform's improved performance and provide robust design strategies for floating offshore wind turbines in deep-water regions, crucial for advancing global renewable energy solutions. Future research should focus on the impacts of different marine conditions on platform performance and consider integrating new materials or innovative design enhancements to further optimize platform functionality. Additionally, due to potential limitations from model simplification, emphasis on real-world testing and validation under operational conditions is recommended. Overall, this research clarifies the differences in structural performance between the T-type and Y-type floating platforms and introduces an improved platform design approach, offering valuable insights and guidance for the future development of floating offshore wind turbine technology.

Keywords: floating offshore wind turbines; floating platforms; structural optimization; structural strength analysis; stability analysis

1. Introduction

Over recent decades, wind energy research has shown a steady rise in capacity. Initially focused on land-based turbines, the industry has faced challenges with noise pollution and aesthetic concerns as turbine sizes increased. This has led to a shift towards offshore wind turbines. These turbines are categorized into two types based on their substructures: fixed and floating. Although 90% of offshore turbines currently use bottom-fixed structures, the limitations in nearshore areas, such as preoccupied optimal locations and impacts on marine fisheries, are notable. Conversely, deep sea regions offer more stable, high-speed wind resources, prompting a move towards to these areas for turbine installation.

In deep sea settings, bottom-fixed offshore wind turbines encounter high installation and maintenance costs, diminishing their economic viability with increasing water depth. This scenario has constrained the development of bottom-fixed turbines. In contrast,

floating structures are better suited for deep-water environments, circumventing seabed topography issues and offering lower installation costs and higher installation efficiency. These advantages position floating offshore wind power as a more viable and sustainable option in deep-sea environments, potentially propelling the advancement of offshore wind power technology.

However, floating offshore wind turbines are usually deployed in waters far from the shore, which makes them inevitably face challenges in extreme environments. Wu et al. [1] proposed a data-driven method to evaluate the fatigue reliability of offshore wind turbines under floating ice loading, demonstrating the importance of incorporating site-specific environmental conditions into structural analysis. Similarly, Dong et al. [2] investigated the fatigue reliability of jacket-supported offshore wind turbines, accounting for corrosion effects and inspection schedules, highlighting the need for robust maintenance strategies. Han et al. [3] extended this work by assessing the multi-axial fatigue behavior of jacket-supported turbines subjected to multiple random correlated loads, providing insights into the complex interactions among various loading conditions. Wu et al. [4] further explored the dynamic responses of monopile offshore wind turbines in cold sea regions, focusing on the combined effects of ice and aerodynamic loads with soil–structure interaction. These studies underscore the importance of detailed structural analyses and the incorporation of complex environmental factors in offshore wind turbine design and optimization. Considering that these devices usually have a design service life of more than 20 years, structural safety issues must be carefully considered during the design and construction process to ensure that floating offshore wind turbines can operate safely and reliably and maintain stability and performance throughout their lifetime. Floating offshore wind turbines float on the sea surface and require anchoring systems to prevent drift and capsizing. In response to this issue, K. Heo et al. [5] conducted numerical simulations to establish motion equations in the frequency domain, studying tilt angles, horizontal movement, and mooring tension under various systems, as well as responses to mooring failures. Safety considerations include stability and structural strength assessments, crucial for both normal and extreme sea conditions. J. Żywicki et al. [6] explored the design of a TLP wind turbine, performing load and motion calculations under extreme conditions and proposing stress calculation methods. S. Wang et al. [7] addressed the non-linearity in floating wind turbine design, validating a method that estimates internal stress for design verification. J. Liu et al. [8] further investigated dynamic response and reliability through time domain simulations, improving long-term response accuracy.

K.R. Hussein et al. [9] developed a method to calculate WindFloat floating foundation components, conducting 3D finite element analysis considering all environmental loads. After safety assessments, structural optimization often follows. Q. Wang [10] enhanced a semi-submersible platform design, optimizing buoyancy, stability, fluid dynamics, and strength. G. Ivanov et al. [11] proposed a hexagonal column structure, analyzing its hydrodynamic performance, stability, and costs. It was mentioned that further studies are needed to explore additional platform shapes and configurations.

I.J. Hsu et al. [12] summarized the design of a 15 MW turbine semi-submersible platform, aiming to optimize the hull structure for cost-effectiveness while meeting strength and stability requirements. They established a relationship between vessel displacement and hull steel weight, providing a foundation for future designs. Most existing research focuses on overall structural loads and motion responses, with limited exploration of internal stresses and torques, highlighting a gap in understanding the response of large platform's internal structures with respect to external loads [13,14].

This study proposes a Y-type offshore wind turbine platform based on an existing T-type offshore wind turbine platform, addressing the critical gaps in the current research, which predominantly focuses on overall structural loads and motion responses but lacks comprehensive analysis of internal stresses and optimization of stiffening members. By systematically comparing various bracing structures, stiffener thicknesses, and stiffening methods, this study demonstrates the advantages of the Y-type platform in reducing von

Mises stress, improving stability under extreme sea state conditions, and optimizing structural weight. Furthermore, through the application of advanced optimization algorithms, this research not only enhances design precision but also achieves significant reductions in material usage, contributing to cost-effective and robust designs for deep-water wind turbine platforms. These contributions extend the existing body of knowledge by integrating detailed internal structural optimization with improved hydrodynamic performance, offering practical insights for the advancement of floating offshore wind turbine technology.

2. Wind Turbine Platform Model

Figure 1 shows the modelling of the floating structures of two offshore wind turbines with different bracing types used in this study, namely T-type and Y-type models. Both models employ the same column and heave plate design, with the only difference being the type of upper bracing connection. Both models have the same column structure, and both have three square columns attached with the same number of bottom heave plates. The bracing is equipped with installation holes for mounting the tower and wind turbine system. Also, both models employ the same internal stiffening arrangement. The column structure has a height of 35 m and a designed draft of 18 m. The principal dimensions of the T-type and Y-type platform models are shown in Table 1.
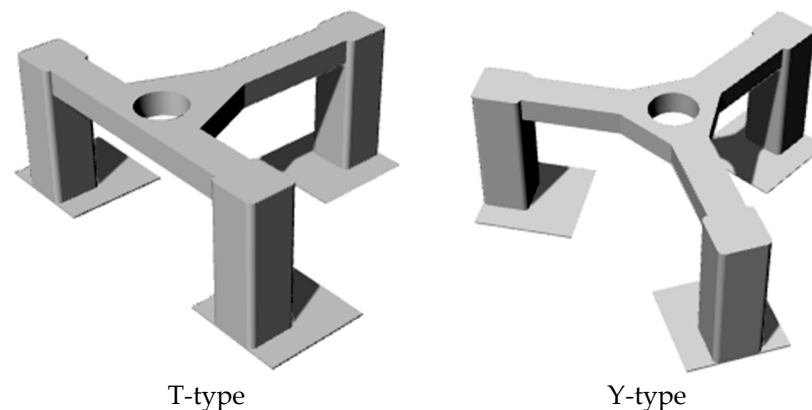
Figure 1. Two different platform models for floating offshore wind turbines.

Table 1. Principal dimensions of the T-type and Y-type floating structures.

Parameters	Unit	Values
Column height	m	35.0
Column wide	m	12.0
Column corner radius	m	1.5
Heave plate breadth	m	25.0
Draft	m	18.0
Displacement	Mega-ton	9363.3

To enhance structural stability and load-bearing capacity, and to maximize resistance to external environmental impacts, ensuring safe and stable operation in designed marine conditions, the column structure utilizes three different types of stiffener sections: L-shape, T-shape and flat-bar configurations. It is noted that, in this study, horizontal stiffeners adopt a flat-bar configuration, while T-shape stiffeners are only employed at the four vertical corners of the column structure and L-shape stiffeners are used for all other vertical directions. Details of the internal stiffener arrangements are shown in Figure 2.
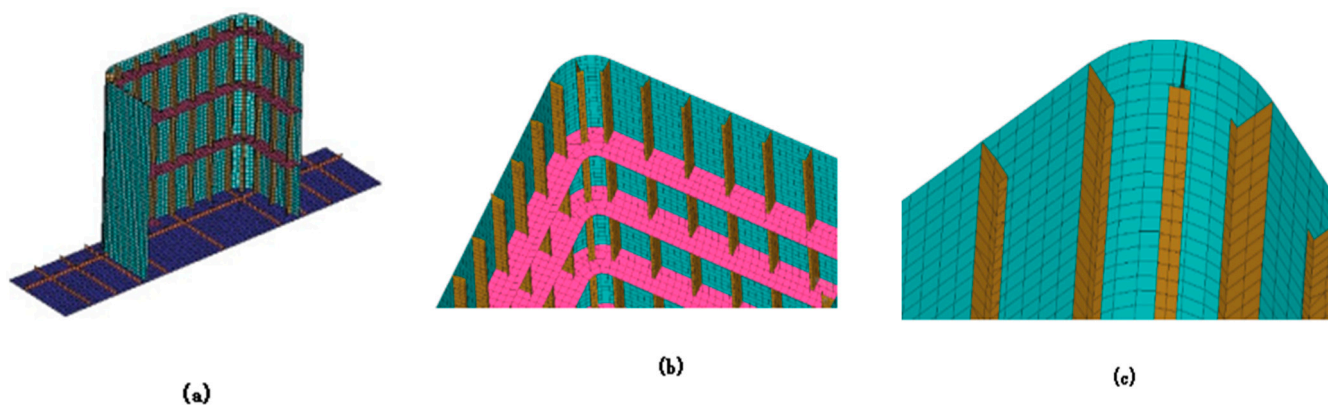
Figure 2. Schematic diagram of the internal stiffeners' arrangement: (**a**) Overall distribution of internal stiffeners including heave plate stiffeners; (**b**) details of internal horizontal and vertical stiffeners; (**c**) details of L-shape and T-shape stiffeners.

Horizontal stiffeners adopt a flat-bar configuration due to their simplicity and effectiveness in resisting lateral forces. This design ensures uniform distribution of stresses across the horizontal plane, improving resistance to shear and preventing buckling under environmental loads. For vertical stiffeners, T-shape stiffeners are placed at the four vertical corners of the column structure, where stress concentrations and torsional effects are most expected. The geometry of T-shape stiffeners provides enhanced resistance to combined bending and torsional loads, which are critical at these high-stress locations. In contrast, L-shape stiffeners are used in other vertical directions to balance structural reinforcement and material usage. These stiffeners offer sufficient bending resistance while minimizing additional weight, contributing to an overall lighter and more efficient design.

The combined use of these three stiffener types offers a well-balanced approach to structural reinforcement. By tailoring the stiffener configuration to the stress distribution characteristics of the column, the design maximizes material utilization and enhances the platform's robustness. This approach ensures that the structure maintains its integrity under extreme wind, wave, and current loads, while also minimizing unnecessary weight, which is crucial for floating offshore wind turbine platforms.

3. Calculation of the External Load

3.1. Weight Acting on the Tower Structure

The proposed semi-submersible offshore wind turbine platform in this study can accommodate up to 9.5 MW wind power generation, and the supporting tower structure is installed at the center of the upper bracing connection part. The information of the wind turbine system considered are provided in Table 2.

Table 2. Information of the wind turbine system (Heo, K. et al., 2023 [5]).

Components	Unit	Values
Blades mass	Mega-ton	105.0
Tower mass	Mega-ton	622.0
Hub mass	Mega-ton	80.0
Nacelle mass	Mega-ton	295.0
Rotor diameter	m	174.0
Hub diameter	m	4.0
Height of the hub from the bottom of tower	m	112.0

3.2. Initial Tension Generated in the Mooring System

The anchoring system used by the T-type and Y-type models adopts a 2 × 3 configuration, as illustrated in Figure 3. This configuration entails one anchor chain connection

point on each of the three columns, with each connection point linking two anchor chains to secure the platform. The anchor chains are connected to the upper outer shell of the floating platform via these connection points.

T-type　　　　　　　　　　　　　　　　Y-type
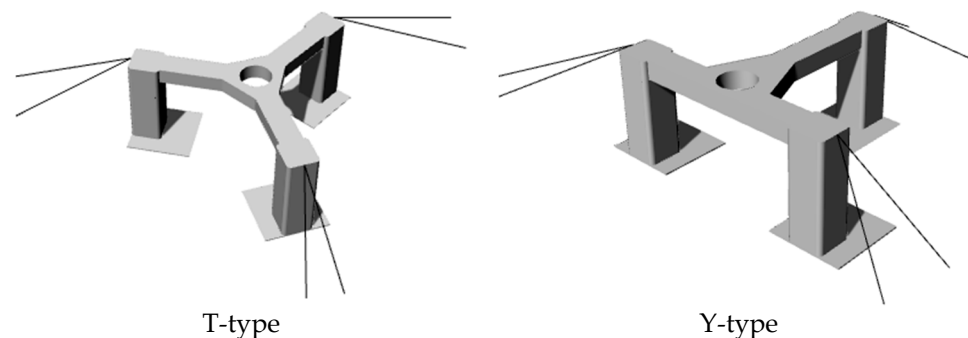
Figure 3. Schematic diagram illustrating the distribution of anchor chains.

The characteristics of the anchoring system are shown in Table 3. The anchoring method commonly used for semi-submersible floating wind turbines is the catenary mooring system. Catenary refers to the curve formed by a uniformly distributed, completely flexible, and non-elongating chain when freely suspended due to the force of gravity. Although the characteristics of the anchor chain for floating foundations are not a perfect match for a pure catenary due to tension and wave effects, the catenary equation is typically employed in the initial design phase of the mooring system due to its computational efficiency.

Table 3. Characteristics of the anchoring system (Heo, K. et al., 2023 [5]).

Parameter	Unit	Value
Type	-	R3 studless
Length	M	900
Diameter	Mm	153
Corrosion allowance	Mm	8
MLB (uncorroded)	kN	16,579
MLB (incl. corrosion)	kN	14,483
Mass per unit of length	kg/m	465
Submerged weight	kg/m	407
Elastic modulus	kN/m^2	5.44×10^7

In the calculation process of the catenary equation, the gravitational force acting on the anchor chain in water can offset the effects of current loads. Therefore, effects, such as flow, inertia forces generated by the anchor chain itself, and elastic deformation, can be ignored. To more accurately study the tension in the anchor chain and the platform's response, the design of the mooring system is divided into preliminary design and detailed design stages. Static analysis calculation methods are often chosen. The following outlines the principles of this analytical approach.

The total tension at any point along the catenary can be decomposed into a horizontal component (T_H) and vertical component (T_V). From the balance equations of horizontal and vertical forces, we can derive the following:

$$T\sin\theta = \omega_1 l = T_V \tag{1}$$

$$T\cos\theta = T_H \tag{2}$$

where ω_1 represents the mass per unit length of the mooring line in water (kg/m).

Considering a differential segment arc length dl along the mooring line, then, Equation (3) is as follows:

$$dT_V = \omega_1 dl \tag{3}$$

Using the geometric relationship between *dl* and *ds* (the arc length along the curve), the following equation for vertical load effect can be derived:

$$dT_V = \omega_1 \sqrt{1 + \left(\frac{dh}{ds}\right)^2}\, ds \tag{4}$$

Since T_V varies with the height of the catenary (*h*), its value can be given by the following Equation (5):

$$T_V = T_H \frac{dh}{ds} \tag{5}$$

where $\frac{dh}{ds}$ represents the slope of the catenary that is the rate of change in height with respect to arc length *s*.

To find out how the vertical tension changes with respect to length, we take the differential of T_V and then integrate the resulting equation along *s*, thus obtaining the following Equation (6):

$$\frac{\frac{d^2 h}{ds^2}}{\sqrt{1 + \left(\frac{dh}{ds}\right)^2}} = \frac{\omega_1}{T_H} \tag{6}$$

Integrating the above equation once again will yield the catenary equation, as follows:

$$h = a\left(\cosh \frac{s}{a} - 1\right) \tag{7}$$

where *a* is the catenary parameter, and it is defined as follows:

$$a = \frac{T_H}{\omega_1} \tag{8}$$

Finally, the tension acting at the upper anchor chain connection point can be expressed as follows:

$$T^2 = T_H{}^2 + T_V{}^2 = T_H{}^2 + (\omega_1 l)^2 \tag{9}$$

3.3. Hydrostatic Pressure Load

Hydrostatic load acts in a direction normal to the contact surface and may arise due to the surrounding water externally or the ballast water located in each column internally. The hydrostatic pressure load to be used is calculated according to the API (American Petroleum Institute)'s RP 2A-LRFD: load and resistance factor design, as follows:

$$P_{hyd} = H_Z \rho_{water} \tag{10}$$

where P_{hyd} is hydrostatic pressure in kg/m^2; ρ_{water} is water density in kg/m^3. H_Z is hydrostatic head in m, and it is defined as follows:

$$H_Z = \bar{d} + \frac{H}{2}\left\{ \frac{\cos k\left(d - \bar{d}\right)}{\cos(kd)} \right\} \tag{11}$$

where $\bar{d}$ is depth below the still water surface including tide when the downward direction is positive in m; *d* is mean water depth in m; *H* is wave height in m; *k* is a parameter representing the propagation characteristics of waves at different water depths.

4. Numerical Modelling

4.1. Internal Stiffening Scheme

To investigate the impact of different internal stiffening arrangement on the structural strength of the floating platform and to find the optimal internal structural design, three

different internal stiffening methods for the T-type and Y-type models are applied (namely cases A, B, and C). Their structural responses are examined and compared. Figure 4 shows these cases and the number of horizontal and vertical stiffeners. In FE model development for the cases, general purpose commercial finite element analysis packages, such as FEGate For Ship, MSC, and Nastran were used to investigate the structural responses of them with the aim of minimizing the total weight of the structures while satisfying the structural design requirement from a strength viewpoint.

Case A (32 × 10)   Case B (32 × 8)   Case C (32 × 6)
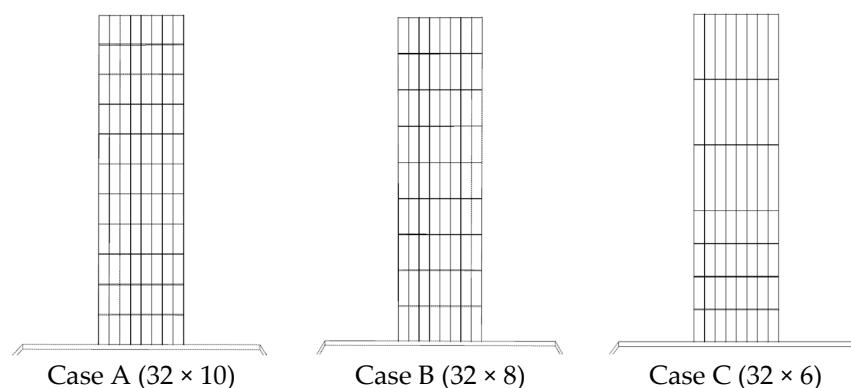
Figure 4. Internal stiffener arrangement of cases A, B, and C.

Details of the differences in the internal stiffening arrangement for the three cases are as follows:

- In case A, each column consists of 32 vertical stiffeners and 10 horizontal stiffeners.
- In case B, each column consists of 32 vertical stiffeners and 8 horizontal stiffeners.
- In case C, each column consists of 32 vertical stiffeners and 6 horizontal stiffeners.

It is important to note that when conducting structural strength analysis, it is essential to consider the safety margin of the selected materials for the T-type and Y-type models. In this study, 355 MPa was initially chosen as the yield strength of AH36 steel. However, as fatigue analysis was not considered, according to the CCS (China Classification Society)'s construction specifications, 301 MPa was chosen as the final maximum yield strength of AH36 steel (see Table 4).

Table 4. Yield strength values of AH36 for different analysis conditions (CCS, 2023 [15]).

Material Yield Strength (MPa)	Static Load Condition (MPa)	Combined Working Conditions and Local High Stress Detailed Fatigue Analysis of Force Points Analysis (MPa)
355	301	312

4.1.1. Structural Analysis Results of Case A

For 32 vertical and 10 horizontal internal stiffeners, their thickness values were varied systematically by considering the principal dimensions of the T-type and Y-type models (see Table 1) with the aim of finding the minimum thickness values while satisfying the structural design requirement (see Table 4). Table 5 shows the combination of the vertical and horizontal stiffener thickness values. Beginning with 35 mm and 60 mm for the vertical and horizontal stiffeners, respectively, their thickness values were then reduced by 6 mm. Afterward, additional stiffener thickness values were introduced by increasing the thickness values by 1 mm to more accurately search the allowable stiffener thickness values.

Table 5. Stiffener thickness variations for the structural analysis of case A.

		Thickness (mm)						
T-type	Vertical stiffeners	35	29	23	17	11	12	13
	Horizontal stiffeners	60	54	48	42	36	37	38
Y-type	Vertical stiffeners	35	29	23	17	11	12	13
	Horizontal stiffeners	60	54	48	42	36	37	38

Figures 5 and 6 show the structural analysis results of case A. For the T-type model, the thickness values of 13×38 mm for the vertical and horizontal stiffeners produced the von Mises stress that is the closest to the structural design requirement. For the Y-type model, the optimal thickness values of 12×37 mm for the vertical and horizontal stiffeners are observed. These differences can be attributed to the distinct geometrical configurations of the two platforms. The Y-type model's bracing system distributes loads more evenly across the structure, resulting in reduced stress concentrations, and allows for the use of slightly thinner stiffeners while maintaining structural integrity.
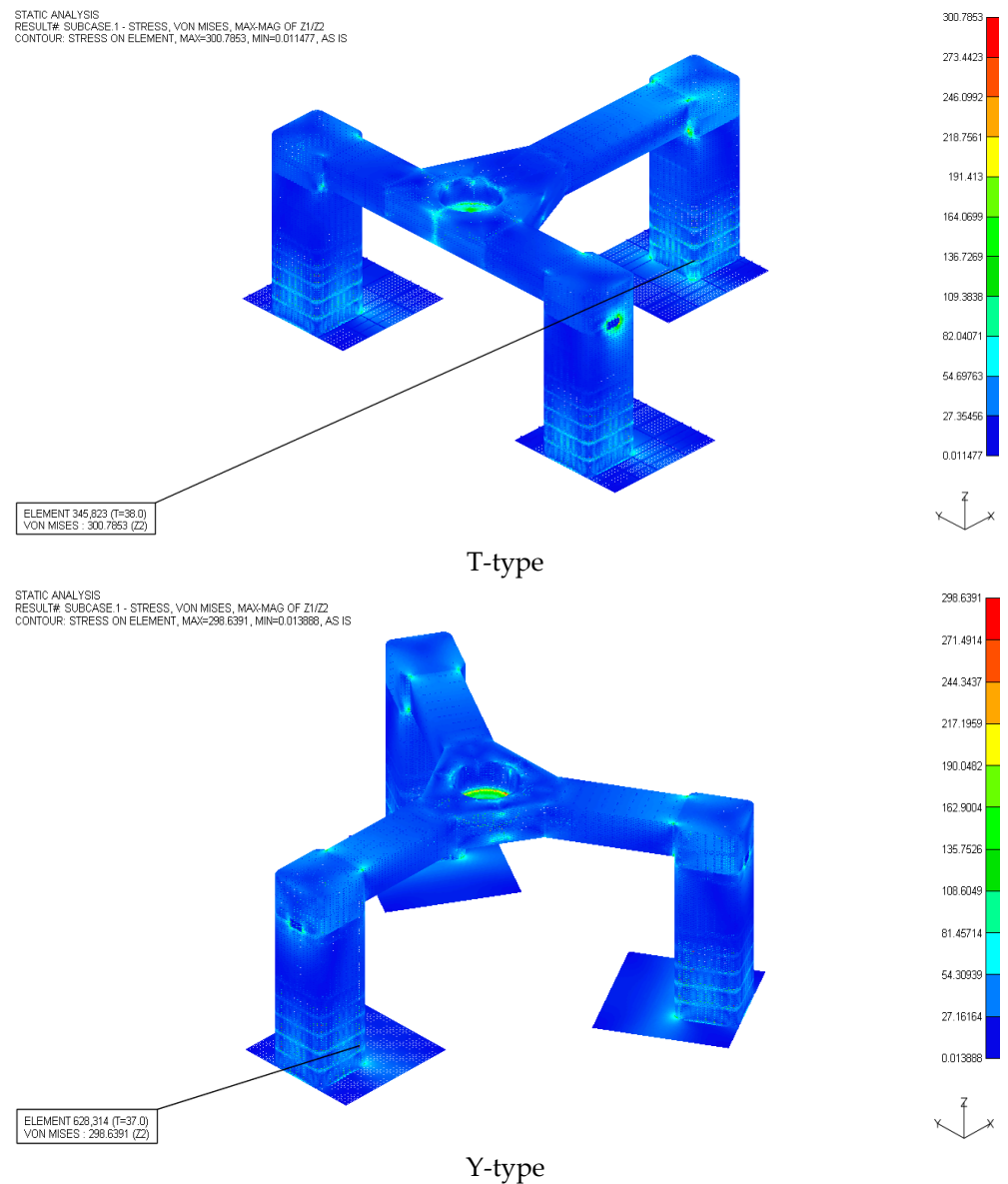
T-type

Y-type

Figure 5. Von Mises stress distribution of the T-type and Y-type models of case A when allowable stiffener thickness values are found.
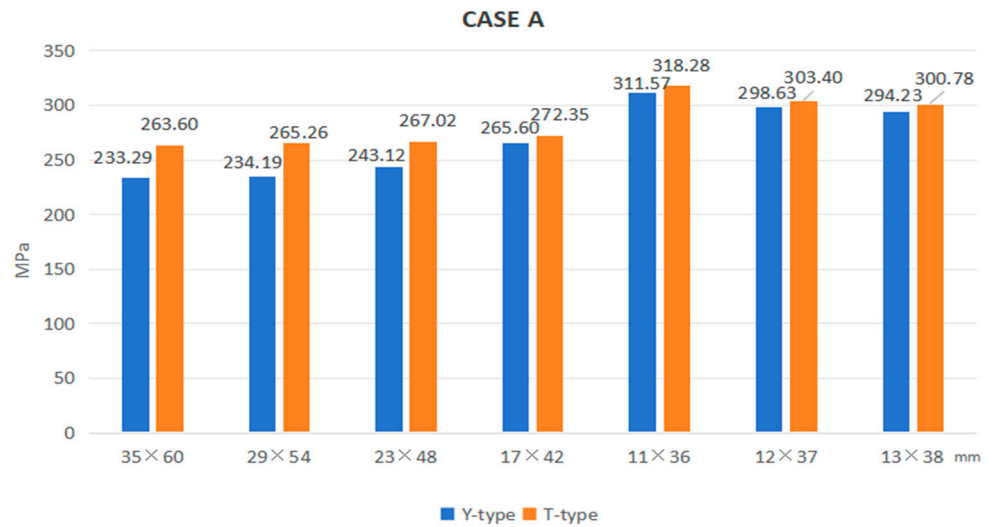
Figure 6. Comparison of von Mises stresses of the T-type and Y-type of case A with respect to the combination of stiffness thickness variations.

These findings highlight the importance of bracing configuration and stiffener thickness optimization in improving the structural performance of floating offshore platforms. By enabling a reduction in material usage without compromising strength, the Y-type model demonstrates superior design efficiency and offers a clear advantage for practical applications in deep-water offshore wind turbine platforms.

In this internal stiffening configuration, von Mises stress of the Y-type model is consistently lower than that of the T-type model, with a maximum difference of 30.21 MPa and a minimum difference of 2.68 MPa indicating an average difference of 15.78 MPa. It is evident that, under all the proposed internal stiffener thickness value combinations, the structural strength performance of the Y-type model is better than that of the T-type model.

4.1.2. Structural Analysis Results of Case B

As in the structural analysis of case A, the thickness values of the 32 vertical and 8 horizontal internal stiffeners were varied systematically by considering the principal dimensions of the T-type and Y-type models (see Table 1) with the aim of finding the minimum thickness values for the stiffeners while satisfying the structural design requirement defined in Table 4. Table 6 shows the combination of the vertical and horizontal stiffener thickness values. Beginning with 35 mm and 60 mm for the vertical and horizontal stiffeners, respectively, the thickness values were reduced by 6 mm down to 17 × 42 mm. Afterward, additional stiffener thickness values were introduced, such as 20 × 45 mm, 21 × 46 mm, and 22 × 47 mm, to more accurately search the allowable stiffener thickness values.

Table 6. Stiffener thickness variations for the structural analysis of case B.

		Thickness (mm)						
T-type	Vertical stiffeners	35	29	23	17	20	21	22
	Horizontal stiffeners	60	54	48	42	45	46	47
Y-type	Vertical stiffeners	35	29	23	17	20	21	22
	Horizontal stiffeners	60	54	48	42	45	46	47

The structural analysis results of case B are shown in Figures 7 and 8. In the case of the T-type model, the thickness values of 20 × 45 mm for the vertical and horizontal stiffeners produce the von Mises stress that is the closest to the structural design requirement. In the case of the Y-type model, the vertical and horizontal stiffener values of 22 × 47 mm show the closest von Mises stress to the structural design requirement.

STATIC ANALYSIS
RESULT#: SUBCASE.1 - STRESS, VON MISES, MAX-MAG OF Z1/Z2
CONTOUR: STRESS ON ELEMENT, MAX=298.2506, MIN=0.00853, AS IS

ELEMENT 360,805 (T=45.0)
VON MISES : 298.2506 (Z2)

T-type

STATIC ANALYSIS
RESULT#: SUBCASE.1 - STRESS, VON MISES, MAX-MAG OF Z1/Z2
CONTOUR: STRESS ON ELEMENT, MAX=300.2104, MIN=0.012856, AS IS

ELEMENT 611,856 (T=47.0)
VON MISES : 300.2104 (Z2)
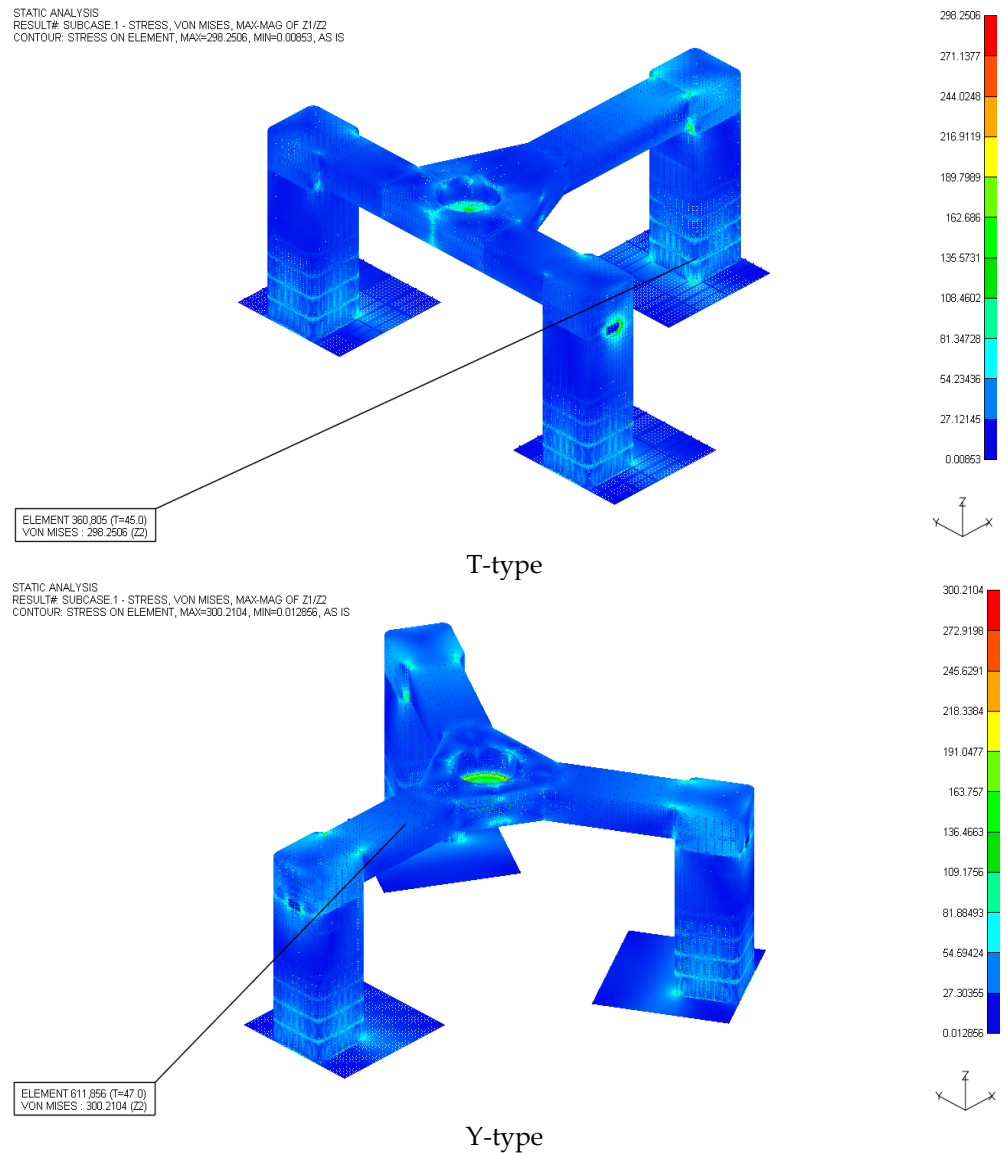
Y-type

Figure 7. Von Mises stress distribution of the T-type and Y-type models of case B when allowable stiffener thickness values are found.
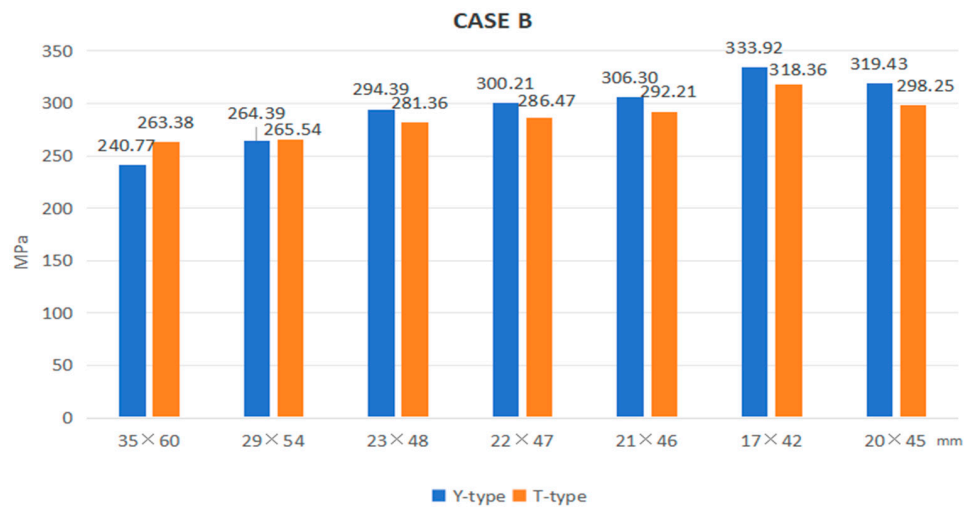
Figure 8. Comparison of von Mises stresses of the T-type and Y-type of case B with respect to the combination of stiffness thickness variations.

In this internal stiffening configuration, as the thickness of the vertical and horizontal stiffeners reduces, the von Mises stress of the Y-type model begins to show greater values than those of the T-type model. Only at the 35 × 60 mm and 29 × 54 mm thickness values does the T-type model show greater von Mises stress than the Y-type model. This observation is thought to be due to the effect of the present regular horizontal stiffener spacing and relatively large stiffener thickness values. From this analysis, the structural strength performance of the T-type model tends to better than that of the Y-type model for the case B internal stiffening arrangement in conjunction with the corresponding stiffener thickness value combination, especially as their von Mises stress values approach the structural design requirement. For these stiffener thickness combinations, the maximum and minimum von Mises stress differences are 21.22 MPa and 13.03 MPa, respectively, with an average difference of 15.53 MPa.

4.1.3. Structural Analysis Results of Case C

Case C's internal stiffening arrangement consists of 32 vertical and 6 horizontal stiffeners. It should be mentioned that the stiffener spacing for the upper part of the column is wider than that for the lower part of the column to consider the location of the water-ballast tank. Based on this, internal stiffener thickness values are varied systematically by considering the principal dimensions of the T-type and Y-type models (see Table 1) with an aim of finding the minimum thickness values while satisfying the structural design requirement described in Table 4. Table 7 shows the combination of the vertical and horizontal stiffener thickness values. As in the previous two cases, the thickness values started at 35 mm and 60 mm for the vertical and horizontal stiffeners, respectively, and then their thickness values were reduced by 6 mm down to 17 × 42 mm. Afterward, additional stiffener thickness values were introduced, such as 16 × 41 mm and 18 × 43 mm, to more accurately search the allowable stiffener thickness values.

Figures 9 and 10 show the structural analysis results of case C. In the case of the T-type model, the thickness values of 18 × 43 mm for the vertical and horizontal stiffeners produce the von Mises stress that is the closest to the structural design requirement. In the case of the Y-type model, the vertical and horizontal stiffener values of 17 × 42 mm show the closest von Mises stress to the structural design requirement.
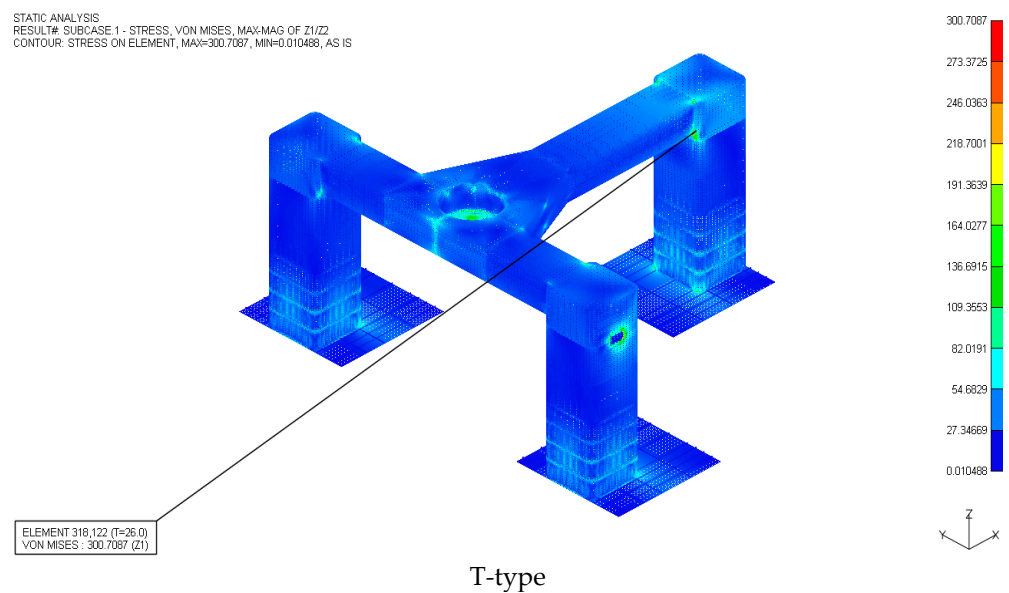
T-type

Figure 9. *Cont.*
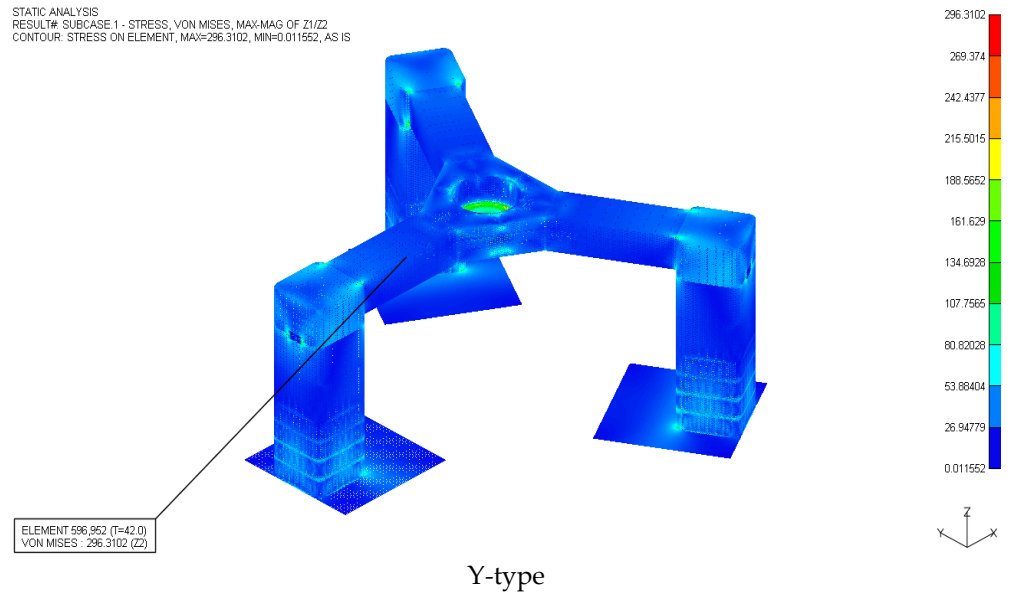
Y-type

Figure 9. Von Mises stress distribution of the T-type and Y-type models of case C when allowable stiffener thickness values are found.
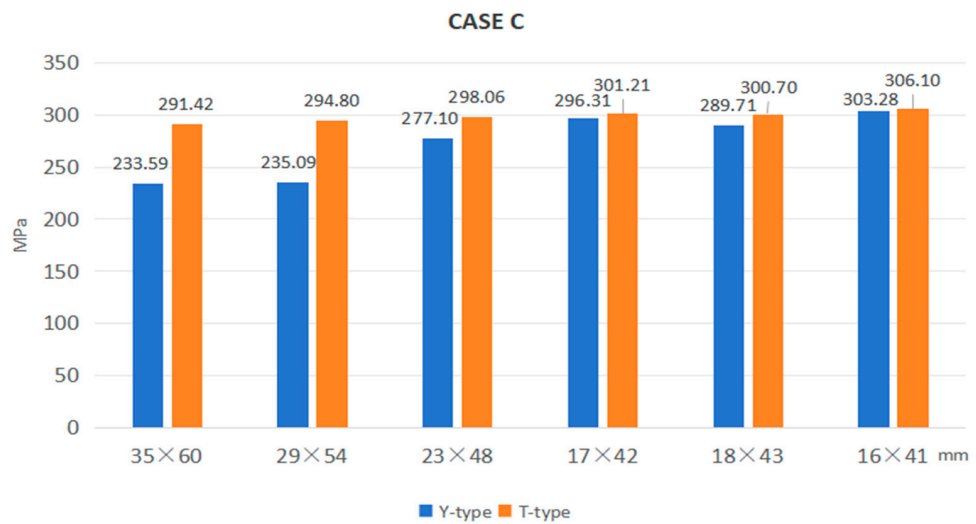
Figure 10. Comparison of von Mises stresses of the T-type and Y-type of case C with respect to the combination of stiffness thickness variations.

Table 7. Stiffener thickness variations for the structural analysis of case C.

		Thickness (mm)					
T-type	Vertical stiffeners	35	29	23	17	18	16
	Horizontal stiffeners	60	54	48	42	43	41
Y-type	Vertical stiffeners	35	29	23	17	18	16
	Horizontal stiffeners	60	54	48	42	43	41

In this internal stiffening configuration, the von Mises stress of the Y-type model is consistently lower than that of the T-type model, with a maximum difference of 59.71 MPa, a minimum difference of 2.82 MPa, and an average difference of 26.20 MPa. It is evident that, under all the proposed internal stiffener thickness value combination and the different stiffener spacings for the upper and the lower part of the column due to the existence of water-ballast tank, the structural strength performance of the Y-type model is better than that of the T-type model.

4.2. Calculation of the Stability of the Two Platform Models

The T-type and Y-type floating offshore wind turbine platforms are different in their structural configurations and, therefore, their hydrodynamic performance. This section aims to investigate the hydrodynamic performance of these two platform models in terms of stability by simulating their 6-degree-of-freedom motions. Through the comparison of the stability of these two models, a better understanding of their hydrodynamic performance can be achieved. The simulation model can provide the accurate motion response of the T-type and Y-type models under the same sea state condition. In this study, a simplified model is used for stability analysis from a quick and economical calculation perspective; thus, the effect of the mooring system is not considered in the simulation. In this respect, the degrees of freedom in sway, roll, surge, and yaw are fixed during the 6-degree-of-freedom calculation for the anchoring effect of the mooring chains attached to the T-type and Y-type models. The stability of the two platform models is, thus, investigated as accurately as possible by considering the heave and pitch motion values. The 6-degree-of-freedom calculation of the two models is performed under the extreme sea state condition representing a 50-year return period in the target offshore area, and a period of 10,800 s is selected as the time domain. The oceanographic parameters for this extreme condition are detailed in Table 8, with the JONSWAP wave model being utilized for wave representation.

Table 8. Parameters of the extreme sea state condition (Y. Yang et al., 2020 [14]).

Return Period (Years)	Significant Wave Height (m)	Peak Period (s)
50	8.14	11.50 ± 1.5

Based on the data from Tables 9 and 10, and Figure 11, under the extreme sea state condition, the Y-type model shows a pitch response amplitude of 21.2562° with an equilibrium position at −0.0225°, and a heave response amplitude of 4.7073 m with an equilibrium position at −0.0443 m, while the T-type model shows a pitch response amplitude of 26.1924° with an equilibrium position at 0.0546°, and a heave response amplitude of 9.0485 m with an equilibrium position at −1.4828 m. In the pitch motion, the maximum value of the Y-type decreases by 2.7447° compared to that of the T-type, while the response amplitude of the Y-type decreases by 4.9362° compared to that of the T-type. In the heave motion, the maximum value of the Y-type decreases by 0.6806 m compared to that of the T-type, while also the response amplitude of the Y-type decreases by 4.3412 m compared to that of the T-type.

Table 9. Statistical analysis of the heave and pitch motion values of the Y-type model.

Motions	Maximum Value	Minimum Value	Response Amplitude	Average Value	Standard Deviation
Pitch	10.6172	−10.6390	21.2562	−0.0225	4.1907
Heave	2.2231	−2.4799	4.7073	−0.0443	0.5763

Table 10. Statistical analysis of the heave and pitch motion values of the T-type model.

Motions	Maximum Value	Minimum Value	Response Amplitude	Average Value	Standard Deviation
Pitch	13.3619	−12.8307	26.1924	0.0546	5.1306
Heave	2.9037	−6.1114	9.0485	−1.4828	1.4143

Based on the analysis results above, although the influence of lateral wave-induced loads on the stability of the two platform models has not been considered, by solely comparing the pitch and heave motion values, it is evident that the Y-type model demonstrates

better stability compared to that of the T-type model. This finding can serve as basic reference material for future research into similar model analyses.
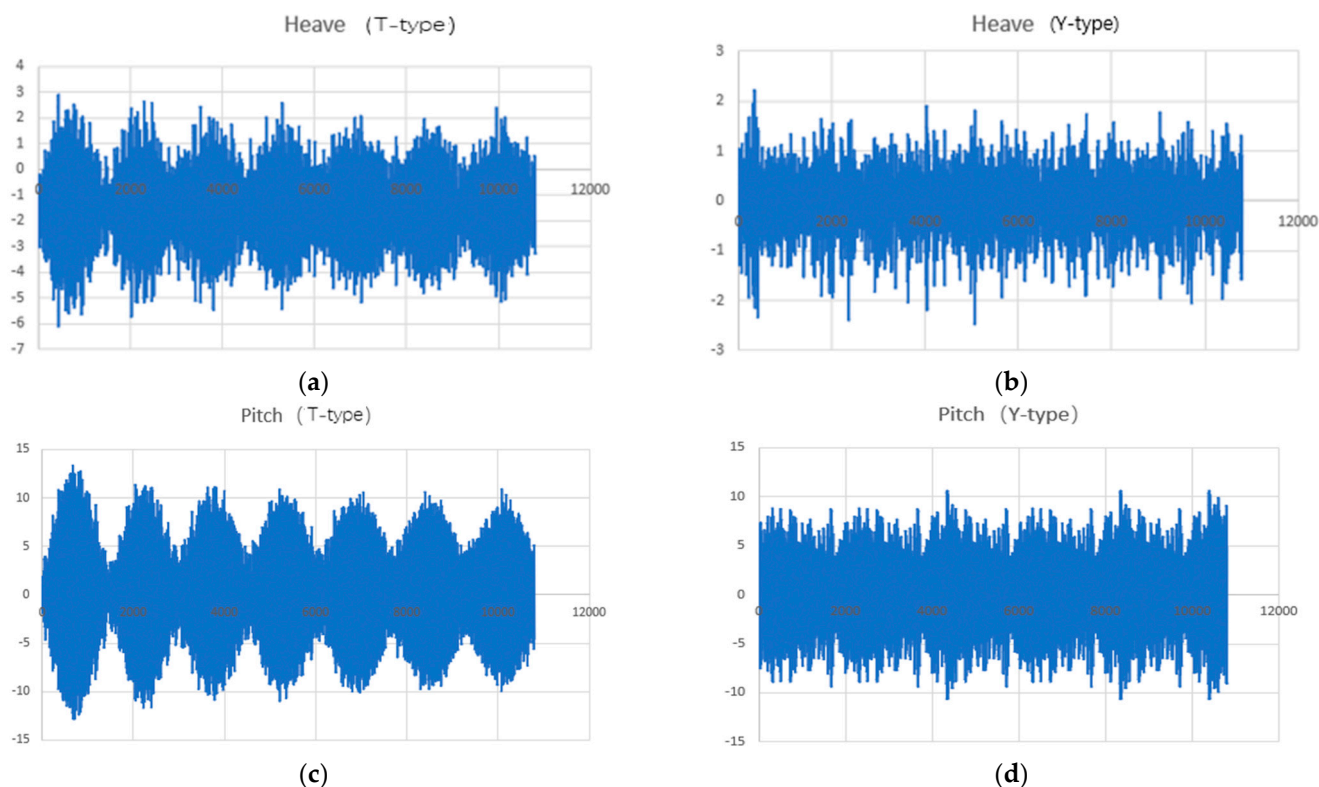
Figure 11. Comparison of the heave and pitch motion values of the T-type and Y-type models.

These improvements can be attributed to the distinct structural design of the Y-type model, particularly its triangular bracing system, which enhances load distribution and overall stiffness. The triangular bracing minimizes the transmission of dynamic forces to the heave plates, leading to reduced vertical displacement and enhanced stability. Additionally, the bracing's geometry introduces a more uniform stress distribution within the columns, decreasing the torsional and bending effects caused by wave-induced loads. This ensures that the Y-type model maintains a more stable equilibrium during extreme conditions. In contrast, the straight bracing of the T-type model results in less efficient load transfer and higher stress concentrations at the column-bracing connections, amplifying the platform's pitch and heave motions. The higher response amplitudes observed in the T-type model highlight its susceptibility to external disturbances, which may compromise its long-term operational reliability under extreme sea state conditions.

While these findings provide valuable insights, it is important to note that the current analysis does not account for lateral wave-induced loads, which may further affect stability. Nevertheless, the results clearly demonstrate the structural advantages of the Y-type model in mitigating pitch and heave motions. This underscores the potential of the Y-type platform as a robust solution for floating offshore wind turbines, particularly in harsh marine environments. Future studies could integrate lateral wave effects and explore additional bracing configurations to further validate and refine these findings.

5. Optimization of the Column Structure of the Platform Models

Optimization Process

In this section, the optimization of the column structure of the platform models is performed by considering the shape and thickness of the internal stiffener and the column shell thickness as parameters to optimize using MSC, Nastran SOL 200 module. Using this Nastran solution module, both the shape and thickness of the inner stiffeners and the thick-

ness of column shells can be optimized satisfying the structural design requirement while minimizing overall weight. Through this process, the structural performance efficiency of the column of the platform models can be enhanced. Figure 12 shows the parameters for the optimization of the column shell and internal stiffener, and the overall optimization process is presented in Figure 13 considering the function of Nastran SOL 200 module.

Figure 12. Details of the optimization parameters.
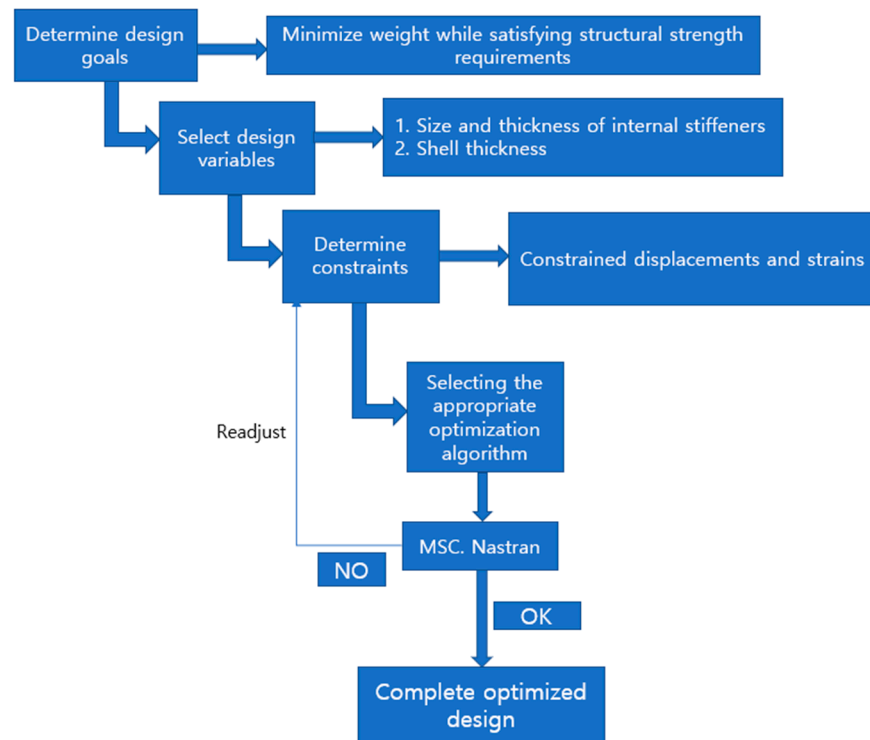
Figure 13. Structural optimization process adopted using the NASTRAN SOL200 module.

During the optimization process, the column structure, including the internal stiffeners, are subjected to re-modelling according to the Nastran SOL 200 algorithm, and the internal stiffener is treated as a beam element. After applying the relevant load and boundary conditions in conjunction with the definition of the optimization parameters, the necessary bulk data file (BDF) is generated for computation, and it is submitted for the Nastran solver for solving. Concerning this, Figures 14 and 15 and Table 11 show the optimization calculation procedure.

Figure 14. Total structural weight and the parameter variation curves during the optimization process.

Table 11. List of design variable history.

	INTERNAL			EXTERNAL				
DV. ID	DV. ID	LABLE	INITIAL	1	2	3	4	5
1	7	P:7	5.0000×10^1	6.7000×10^1	1.0000×10^1	1.3500×10^1	1.0000×10^1	1.2500×10^1
2	8	L1:8	4.0000×10^2	5.0000×10^2	5.0000×10^2	5.0000×10^2	5.0000×10^2	5.0000×10^2
3	9	L2:9	1.0000×10^2	1.0371×10^2	1.2030×10^2	1.2393×10^2	1.2500×10^2	1.2500×10^2
4	10	L3:10	2.0000×10^1	1.8422×10^1	1.3560×10^1	1.8274×10^1	2.0134×10^1	2.5168×10^1
5	11	L4:11	2.0000×10^1	3.3714×10^1	3.5000×10^1	3.5000×10^1	3.5000×10^1	3.5000×10^1
6		7	8	9	10	11	12	13
1.0000×10^1		1.1250×10^1	1.2656×10^1	1.1074×10^1	1.1766×10^1	1.1031×10^1	1.1376×10^1	1.1731×10^1
5.0000×10^2		5.0000×10^2	5.0000×10^2	5.0000×10^2	5.0000×10^2	5.0000×10^2	5.0000×10^2	5.0000×10^2
1.2500×10^2		1.2500×10^2	1.2500×10^2	1.2500×10^2	1.2500×10^2	1.2500×10^2	1.2500×10^2	1.2500×10^2
2.6835×10^1		3.0190×10^1	3.3964×10^1	3.5000×10^1	3.5000×10^1	3.5000×10^1	3.5000×10^1	3.5000×10^1
3.5000×10^1		3.5000×10^1	3.5000×10^1	3.5000×10^1	3.5000×10^1	3.5000×10^1	3.5000×10^1	3.5000×10^1

Figure 15. Von Mises stress distribution of design-3.

Analysis of the optimization results reveals that design-3, listed among the design numbers in Table 11, is the optimized design closest to the structural design requirement of 301 MPa. At this point, the maximum von Mises stress of the column structure is calculated as 301.19 MPa, as shown in Figure 15. Although design-3 does not yield the lowest overall weight, it represents the design most compliant with the structural strength requirement. Therefore, for safety considerations, design-3 is selected as the best solution for this optimization design.

The optimized structural parameters obtained for design-3 are shown in Table 12. Based on these parameter values, the total weight of the single column structure adopted in the T-type and Y-type models is calculated, and the result is compared with that of the same column structure without the optimization consideration. The comparison results are presented in Table 13.

Table 12. Optimized structural parameter values.

Parameters	Before Optimization	After Optimization
P	67 mm	15 mm
L1	500 mm	500 mm
L2	125 mm	123.9 mm
L3	35 mm	18.2 mm
L4	35 mm	35 mm

Table 13. Comparison of total structural weight before and after optimization per single column.

	Total Weight (Tons)
Before optimization	3356.04
After optimization	2976.23

This comparison demonstrates that the column structure achieves a weight reduction of 379.81 tons after the optimization, representing an approximately 11.31% reduction in the structural weight. The weight reduction achieved through optimization is primarily due to the targeted adjustment of the stiffener and shell thicknesses, which ensures that materials are used efficiently in regions with higher stress concentrations. The Nastran SOL 200 module prioritizes minimizing excess material in low-stress areas while maintaining adequate reinforcement in critical regions. For example, the optimization process balances the trade-off between shell thickness and stiffener dimensions, ensuring that the column

structure resists bending, torsion, and axial loads effectively without unnecessary overdesign. This systematic approach results in a lighter yet robust design, reducing construction costs and improving buoyancy characteristics, which are crucial for floating offshore wind turbine platforms.

Moreover, the optimization validates the feasibility of using beam elements to approximate internal stiffeners, which simplifies computational requirements without compromising result accuracy. This demonstrates the practical applicability of the Nastran SOL 200 optimization framework for similar large-scale offshore structures. By ensuring that the optimized design meets both weight and strength criteria, the study provides a valuable reference for future developments in the field.

6. Conclusions

In this study, the detailed numerical analyses of the structural strength and dynamic responses of the T-type and Y-type floating platform models are conducted. Comprehensive analysis results indicate that the Y-type model exhibits better stability and lower stress concentration than those of the T-type model in most numerical simulation conditions. Specifically, the Y-type model achieves a maximum reduction in von Mises stress by 30.21 MPa compared to the T-type model under similar design configurations of the internal stiffeners. Additionally, when the pitch and heave motion values of the two models are investigated under extreme sea state conditions, the Y-type model demonstrates better stability, with reductions in pitch and heave motion amplitudes of 4.9362° and 4.3412 m, respectively.

Furthermore, the structural optimization algorithm based on the NASTRAN SOL200 module is applied to the column structure of the T-type and Y-type models to obtain optimal design parameters with the purpose of achieving the minimum structural weight while satisfying the structural strength requirement. The optimization process results in a weight reduction of 11.31% for the column structure, significantly improving the design quality while maintaining strength and durability. The optimization calculations not only successfully reduce the structural weight but also provide rational scantlings of the structural members of the column structure.

The results obtained from this study clarify the differences in structural performance between the T-type and Y-type models and provide practical application values. The Y-type model demonstrates superior performance in terms of stability, structural strength, and material usage, offering a simple but rational design solution for the development of floating offshore wind turbine platforms in deep water, crucial for the advancement of global renewable energy.

As a future research direction, it is recommended to consider the various section shapes of the internal stiffeners as well as additional bracing types connecting the multiple column structures in conjunction with all the 6-degree-of-freedom motions simultaneously to expand the current research findings further.

Author Contributions: The individual contributions of all the co-authors are provided as follows: Conceptualization, H.Y.D., H.K.J. and J.L.J.; methodology, H.Y.D. and H.K.J.; software, H.Y.D. and J.L.J.; validation, H.Y.D. and H.K.J.; formal analysis, H.Y.D.; data curation, H.Y.D.; writing—original draft preparation, H.Y.D.; writing—review and editing, H.K.J.; visualization, H.Y.D.; supervision, H.K.J. All authors have read and agreed to the published version of the manuscript.

Data Availability Statement: The original contributions presented in the study are included in the article, further inquiries can be directed to the corresponding author.

Conflicts of Interest: The authors declare no conflicts of interest.

References

1. Wu, T.; Yang, H.; Wang, P.; Zhang, C.; Zhang, M. Data-driven fatigue reliability evaluation of offshore wind turbines under floating ice loading. *J. Struct. Eng.* **2024**, *150*, 05024004. [CrossRef]
2. Dong, W.; Moan, T.; Gao, Z. Fatigue reliability analysis of the jacket support structure for offshore wind turbine considering the effect of corrosion and inspection. *Reliab. Eng. Syst. Saf.* **2012**, *106*, 11–27. [CrossRef]
3. Han, C.; Liu, K.; Ma, Y.; Qin, P.; Zou, T. Multiaxial fatigue assessment of jacket-supported offshore wind turbines considering multiple random correlated loads. *Renew. Energy* **2021**, *169*, 1252–1264. [CrossRef]
4. Wu, T.; Zhang, C.; Guo, X. Dynamic responses of monopile offshore wind turbines in cold sea regions: Ice and aerodynamic loads with soil-structure interaction. *Ocean. Eng.* **2024**, *292*, 116536. [CrossRef]
5. Heo, K.; Park, H.; Yuck, R.-H.; Lee, D. Numerical investigation of a Floating-Type support structure (Tri-star Floater) for 9.5 MW wind turbine generators. *Energies* **2023**, *16*, 7961. [CrossRef]
6. Żywicki, J.; Dymarski, P.; Ciba, E.; Dymarski, C. Design of structure of tension leg platform for 6 MW offshore wind turbine based on FEM analysis. *Polish Marit. Res. Spec. Issue* **2017**, *230*, 241. [CrossRef]
7. Wang, S.; Xing, Y.; Balakrishna, R.; Shi, W.; Xu, X. Design, local structural stress, and global dynamic response analysis of a steel semi-submersible hull for a 10-MW floating wind turbine. *Eng. Struct* **2023**, *291*, 11674. [CrossRef]
8. Liu, J.; Thomas, E.; Goyal, A.; Manue, L. Design loads for a large wind turbine supported by a semi-submersible floating platform. *Renew Energy* **2019**, *138*, 923–936. [CrossRef]
9. Hussein, K.R.; Hussein, A.W.; Hegazy, E.H.; Amin, A.A. Structural design of a floating foundation for offshore wind turbines in red sea. *Anal. Des. Mar. Struct* **2013**, *17*, 164–174. [CrossRef]
10. Wang, Q. *Design of a Steel Pontoon-Type Semi-Submersible Floater Supporting the DTU 10MW Reference Turbine*; Norwegian University of Science and Technology: Trondheim, Norway, 2014.
11. Ivanov, G.; Hsu, I.-J.; Ma, K.-T. Design considerations on Semi-Submersible columns, bracings and pontoons for floating wind. *Mar. Sci. Eng.* **2023**, *11*, 1663. [CrossRef]
12. Hsu, I.-J.; Ivanov, G.; Ma, K.-T.; Huang, Z.-Z.; Wu, H.-T.; Huang, Y.-T.; Chou, M. Optimization of Semi-Submersible Hull Design for Floating Offshore Wind Turbines. *OMAE* **2022**, *86*, 751.
13. Park, S.; Choung, J. Structural Design of the Substructure of a 10 MW Floating Offshore Wind Turbine System Using Dominant Load Parameters. *J. Mar. Sci. Eng.* **2023**, *11*, 1048. [CrossRef]
14. Yang, Y.; Bashir, M.; Wang, J.; Michailides, C.; Loughney, S.; Armin, M.; Hernández, S.; Urbano, J.; Li, C. Wind-wave coupling effects on the fatigue damage of tendons for a 10 MW multi-body floating wind turbine. *Ocean Eng.* **2020**, *217*, 107909. [CrossRef]
15. China Classification Society (CCS). *Rules for Classification of Steel Ships (2023)*; China Classification Society: Beijing, China, 2023.